

MHD Equilibrium Reconstruction Using the Visible Light Tomographic Method with Laplacian Eigenfunction^{*)}

Kosuke SUZUKI, Sadayoshi MURAKAMI, Satoshi OHDACHI¹⁾,
Hiroshi IDEI²⁾, Kengoh KURODA²⁾, Ryuya IKEZOE²⁾ and Takumi ONCHI²⁾

Kyoto University, Kyoto 615-8540, Japan

¹⁾*National Institute for Fusion Science, Toki 509-5292, Japan*

²⁾*The Research Institute for Applied Mechanics, Kyushu University, Kasuga 816-8580, Japan*

(Received 16 November 2020 / Accepted 3 June 2021)

A tomographic method using tangential visible light is proposed for MHD equilibrium reconstruction via two processes. The first process is a tomographic method to estimate the last-closed-flux-surface (LCFS) in two-dimensional poloidal cross-section using a single tangential camera image. Applying the Laplacian eigenfunction series expansion and L_1 regularization, we can reconstruct the LCFS from relatively sparse and noisy observations. The second method is a free-boundary tokamak equilibrium calculation using the TASK/EQU code, in which we use the estimated plasma surface information as the constraints for the equilibrium calculation. As a result, we develop a new method for identifying equilibrium states using visible light information.

© 2021 The Japan Society of Plasma Science and Nuclear Fusion Research

Keywords: equilibrium, tomography, series expansion, Laplacian eigenfunction, L_1 regularization

DOI: 10.1585/pfr.16.2402090

1. Introduction

Reconstruction of the magnetohydrodynamics (MHD) equilibria from experimental data is the basis for the analysis of tokamak physics. The MHD equilibrium reconstruction is also crucial for plasma shape control and supporting plasma operation. Thus, a quick and accurate equilibrium reconstruction method is required for the future burning plasma experiments like ITER.

The MHD equilibrium reconstruction is commonly performed by analyzing external magnetic measurement data. In a pioneering work, a fast method for reconstructing the equilibrium using external magnetic measurements was proposed by Swain and Neilson [1]. This method uses the least-squares determination of the plasma boundary and a global force balance. Luxon and Brown [2] subsequently developed a more accurate approach in which the best-fit current density profile is established by solving the Grad-Shafranov equation based on external magnetic measurements. This method can determine the characteristic parameters of the plasma current profile and the shape of the plasma cross-section. Because Luxon and Brown's method requires iteratively calculating a non-linear partial equation, it is computationally expensive. The success of these equilibrium reconstruction methods leads to the equilibrium fitting code (EFIT) proposed by Lao *et al.* [3]. This method can efficiently reconstruct the current profile parameters, plasma shapes, and current density profile based on the Picard linearization scheme, which reduces

the computational cost.

However, these reconstructed results have uncertainties because of the errors associated with the observations and computational models utilized because these methods indirectly reconstruct the internal state of the plasma using the observed data. The external coils are located outside the toroidal magnetic field coils at a large distance from the plasma in large-scale fusion devices like ITER. Thus, accurate reconstruction of the plasma equilibrium is becoming more difficult than the devices with external coils near the plasma. If we can estimate the shape of the last-closed-flux-surface (LCFS) using an alternative method, the equilibrium reconstruction performance could be improved.

Tomography can be used to reconstruct the LCFS without solving the Grad-Shafranov equations. Tomography has been used as a plasma diagnostics tool [4]; this methodology can determine the inner plasma profile on a poloidal cross-section using observations from outside the plasma. This poloidal cross-section profile is obtained by solving the inverse problem based on the observations of radiation detectors on the fusion device.

In this work, we utilize tomographic techniques to reconstruct the visible light emission profile on the poloidal cross-section from a single camera image. After having obtained the emission profile, we can easily estimate the shape of the LCFS under the assumption that the H_α emission is radiated from just inside the LCFS. This will be shown in Fig. 8 of QUEST experiment. At the center of the plasma, the H_α emission is weak because the plasma is completely ionized owing to the high temperature. By con-

author's e-mail: suzuki.kosuke.23x@st.kyoto-u.ac.jp

^{*)} This article is based on the presentation at the 29th International Toki Conference on Plasma and Fusion Research (ITC29).

trast, just inside the LCFS, there is a H_α emission due to the excitation of neutral particles entering the plasma from the outside; a localized emission is therefore expected in a thin region near the LCFS.

Tomographic inversion is an essentially ill-posed problem. The series expansion method using orthogonal basis patterns was proposed by Y. Nagayama *et al.* [5]. In that work, the emissivity profile expansion was introduced into the Fourier-Bessel series, and the coefficients were determined by the least-squares-fitting method. K. Yamasaki *et al.* [6] proposed a method to optimize the Fourier-Bessel expansion coefficients precisely. S. Ohdachi *et al.* [7] compared the basis patterns between the Fourier-Bessel and Laplacian eigenfunction and showed the validity of the L_1 regularization.

In this study, we propose a new method to reconstruct the MHD equilibrium starting from a single tangential view camera image using the tomographic technique, and we apply this method to data from QUEST. Like most other instruments, the target device QUEST spherical tokamak [8] has a tangential visible light camera to observe the entire torus plasma. First, we estimate the LCFS of torus plasma using tomography based on an observation from a tangential camera. Then, we select some points on the LCFS where the magnetic flux $\psi = 0$. We then calculate the Grad-Shafranov equation using the TASK/EQU code using these points as the boundary conditions. This method is considered more useful because the LCFS is used as the boundary conditions, whereas the conventional method is based on magnetic measurements on the reactor wall.

This paper is organized as follows. In Section 2, the orthogonal function, which is valuable for the composition of the emission distribution, will be introduced. Second, the proposed method is used to reconstruct the local emission distribution from a single camera image from a tangential direction. Both synthetic and experimental data are used for this test (Section 3). Finally, in Section 4, using the reconstructed local emission, the poloidal magnetic fields are calculated numerically using the equilibrium code.

2. Tomography Using an Orthogonal Basis

In this section, we describe the tomographic reconstruction technique. Tomography is the problem of determining the poloidal cross-sectional emissivity, $f(\mathbf{r}')$, from the tangential observed image, $g(\mathbf{r})$, as shown schematically in Fig. 1. Here, we define \mathbf{r}' as the coordinates in real space and \mathbf{r} as the coordinates on the camera screen. The function $g(\mathbf{r})$ is defined to obey

$$g(\mathbf{r}) = \int_D h(\mathbf{r}, \mathbf{r}') f(\mathbf{r}') d\mathbf{r}', \quad (1)$$

where D is the region of an object's existence and $h(\mathbf{r}, \mathbf{r}')$ represents a projection coefficient of \mathbf{r}' to \mathbf{r} . With column

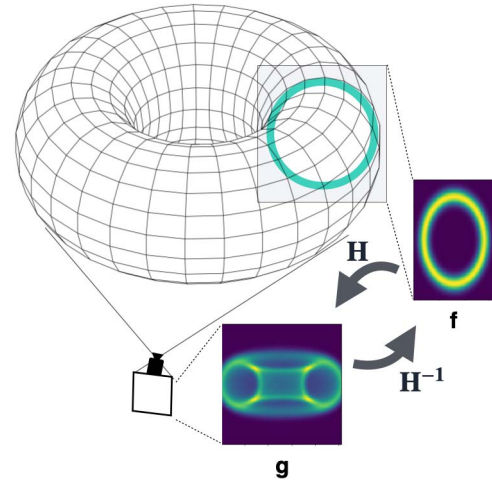


Fig. 1 Schematic view of the tomographic reconstruction.

vectors \mathbf{f} and \mathbf{g} , Eq. (1) can be expressed as a discrete equation:

$$H\mathbf{f} = \mathbf{g}$$

$$H = \begin{bmatrix} h_{11} & h_{12} & \cdots & \cdots & h_{1N} \\ h_{21} & h_{22} & \cdots & \cdots & h_{2N} \\ \vdots & \vdots & & & \vdots \\ h_{M1} & h_{M2} & \cdots & \cdots & h_{MN} \end{bmatrix}, \quad (2)$$

$$\mathbf{f} = \begin{bmatrix} f_1 \\ f_2 \\ \vdots \\ \vdots \\ f_N \end{bmatrix}, \quad \mathbf{g} = \begin{bmatrix} g_1 \\ g_2 \\ \vdots \\ g_M \end{bmatrix} \quad (N, M \in \mathbb{N}).$$

Here we define $h_{mn} = h(\mathbf{r}_m, \mathbf{r}'_n) \Delta\mathbf{r}'_n$, $f_n = f(\mathbf{r}'_n)$, $g_m = g(\mathbf{r}_m)$. Figure 1 shows a schematic of the interpretation of Eq. (2). We reconstruct \mathbf{f} from \mathbf{g} by applying the inverse operator H^{-1} . However, this inversion problem presents an ill-posed and often under-determined problem because fusion plasma data are usually spatially sparse because of the limited number of detectors. In other words, the inverse matrix H^{-1} cannot be computed because H is not a matrix with full rank.

Here, we use the tangential view of the whole torus as \mathbf{g} . In devices larger than QUEST, it is expected that the observed image will be limited to one side of torus. In tokamaks, because toroidal axial symmetry is assumed, there is no significant effect if the poloidal cross section is covered. However, if there is inherent noise at a particular location, it will affect the reconstructed image as the noise cannot be smoothed in the toroidal direction.

In this case, the most basic approach to solving Eq. (2) is using the least-squares method. This method gives the solution \mathbf{f} minimizing the following equation

$$\mathbf{g} = \arg \min_{\mathbf{g}} |\mathbf{g} - H\mathbf{f}|. \quad (3)$$

Because this solution is often under-determined and unsta-

ble, an additional penalty term is used. The total magnitude of the local emission is used as a penalty term, and the function to be minimized becomes

$$\mathbf{g} = \arg \min_{\mathbf{g}} |\mathbf{g} - H\mathbf{f}| + \lambda |\mathbf{g}|_{\alpha}. \quad (4)$$

When $\alpha = 2$, the penalty function is the Euclid norm of the vector \mathbf{g} .

$$|\mathbf{g}|_2 = \sqrt{g_1^2 + g_2^2 + \dots + g_N^2}. \quad (5)$$

This method is called L_2 regularization (Ridge regression) and suppresses the magnitude of the solution. When $\alpha = 1$, the penalty function is the sum of the absolute values of each term:

$$|\mathbf{g}|_1 = |g_1| + |g_2| + \dots + |g_N|. \quad (6)$$

This method is called L_1 regularization or, least absolute shrinkage and selection operator, (LASSO regression) [9]. LASSO regression shrinks some coefficients to zero. Hence, it tends to retain a reasonable basis. If the matrix H is orthogonal, LASSO linear regression can be optimized efficiently using the LARS [10] algorithm.

A local emission distribution approximated as series expansion, by contrast, makes the linear equation small, and then it is possible to derive a solution even from sparse observations. In the series expansion method, the local emissivity \mathbf{f} can be expanded as a series of patterns \mathbf{b}_i :

$$\mathbf{f} = \sum_i a_i \mathbf{b}_i. \quad (7)$$

Substituting Eq. (7) into Eq. (2), and replace the basis patterns as $\mathbf{B}_i = H\mathbf{b}_i$ gives the following:

$$\mathbf{g} = \sum_i a_i H\mathbf{b}_i = \sum_i a_i \mathbf{B}_i. \quad (8)$$

Each coefficient a_i can be optimized according to

$$a_i = \arg \min_{a_i} |g_i - a_i \mathbf{B}_i| + \lambda |a_i|_{\alpha}. \quad (9)$$

Having obtained a_i , we can easily calculate the reconstructed image \mathbf{f} using Eq. (7).

The Fourier basis is generally used in image processing as a series expansion approximation of an image. In this study, we introduce a basis that is more suitable for the plasma emission distribution.

Here we use the Laplacian eigenfunctions (LEs) as a basis. Consider the fundamental solution of the Laplacian in two dimensions,

$$K(x, y) = -\frac{1}{2\pi} \log |x - y|, \quad (10)$$

this operator K has the following eigenfunction expansion

$$K(\mathbf{x}, \mathbf{y}) \sim \sum_{j=1}^{\infty} \mu_j \varphi_j(\mathbf{x}) \overline{\varphi_j(\mathbf{y})}. \quad (11)$$

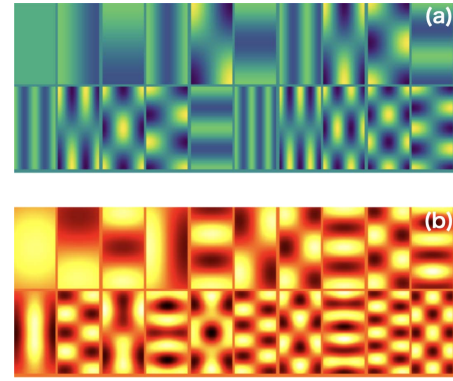


Fig. 2 Basis patterns of series expansion (first 20 patterns). (a) Fourier basis and (b) LE basis.

This eigenvector ϕ constitutes an orthogonal basis. Figure 2(b) shows the LE basis. The Fourier basis (Fig. 2(a)) is a commonly used method to approximate images by series expansion. The Fourier basis is incompatible with the representation of aperiodic local emissions because it implicitly assumes a periodic boundary condition. However, the LE basis is considered to be suitable for constructing the local emission profile observed in fusion plasma. As the plasma is a continuum, it is expected to be reconstructed using a low-mode basis (a basis with gradual changes).

3. Application to the Tangential Viewing System of QUEST

In this section, we demonstrate the application of the proposed method to the tangential viewing system of QUEST. Reconstruction of the local emission profile from a synthetic or experimental tangential image will be discussed. Figure 3 shows the arrangement of the virtual tangential camera system of QUEST. This camera observes the torus plasma, which has a circular cross-section.

First, we try to reconstruct the local emission from the synthetic image with noises as a test. Figure 4(a) is the synthetic observation image, which is added uniform Gaussian noises and synthetic reflective objects (center vertical bar and horizontal square dots) have been added. (e) shows the ground truth. Figures 4(b-d) show a comparison of the results of the three methods. Figure 4(b) shows the results of the L_2 regularized least-squares method of Eq. (4), Fig. 4(c) shows the results of the reconstruction using the Fourier basis, and Fig. 4(d) shows the reconstruction obtained using the LE basis. The orthogonal basis approaches (Figs. 4(c and d)) achieve a much cleaner reconstruction than the results obtained using the L_2 regularized least-squares method. Little difference can be observed between the results of the Fourier and LE basis methods shown in Figs. 4(c) and (d), respectively, because both use 1000 patterns. This number is sufficient for both bases to reconstruct the image well. However, a more prefer-

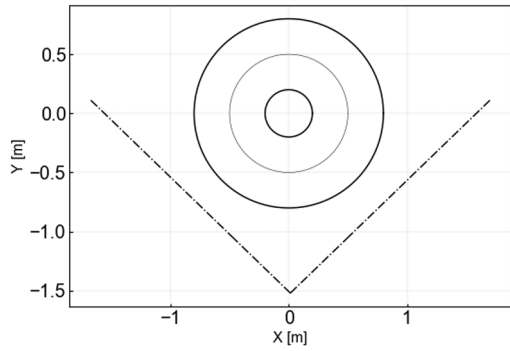


Fig. 3 Schematic view of QUEST plasma (top). The inner and outer bold lines represent the boundaries of the area where plasma can exist.

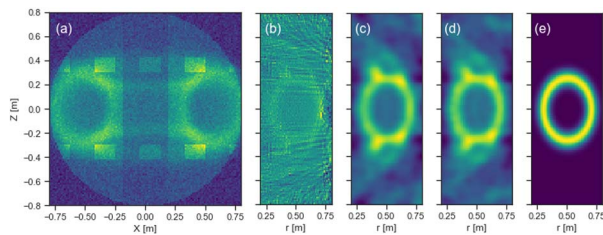


Fig. 4 (a) A synthetic tangential image with uniform Gaussian noise and synthetic object noise. (b) Reconstruction results using the L_2 regularized least-squares method. (c) Reconstruction results using a Fourier basis. (d) Reconstruction using a LE basis. (e) Ground truth.

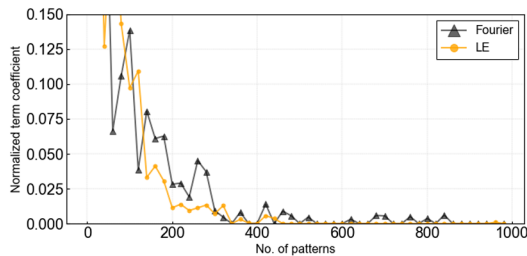


Fig. 5 Absolute values of cumulated every 20 coefficients a_i , which represents the strength of each basis term. Black line is the Fourier basis coefficients, and yellow line is the LE basis coefficients. For comparison, each value is normalized by the maximum value.

able basis can reconstruct the cross-sectional profile using a smaller number of patterns. In the following, we evaluate the suitability of these bases.

We compare each of the coefficients a_i in Eq. (7) in the cases of using 1000 patterns. Figure 5 shows the normalized absolute values of each coefficient a_i . Figure 5 shows that the LE basis has small values of a_i for $i > 200$, whereas the Fourier basis uses some large values of a_i even for larger i . This indicates that a low-mode LE basis can encode the local emission more efficiently than can the Fourier basis, and that it is therefore more compatible with plasma reconstruction.

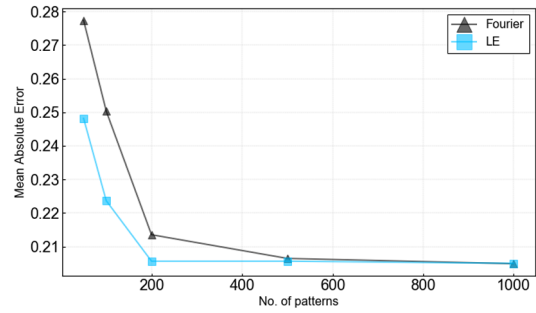


Fig. 6 Mean absolute errors between the reconstructed image and the ground truth. LE method's error decrease faster than Fourier method.

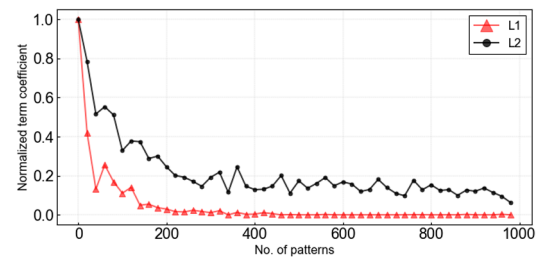


Fig. 7 The cumulated values for every 20 patterns of normalized absolute coefficients. Black line is L_2 regularization and red line is L_1 regularization. For comparison, each value is normalized by the maximum value.

Here, we compare the performances of the Fourier and LE bases by varying the number of patterns used. Figure 6 shows the mean absolute error of the two methods and its dependence on the number of patterns. We can see that the LE method reaches stable value at $i = 200$. When a sufficiently large number of patterns are used (approximately over 500), there is little difference between these two methods. By contrast, when a low number of patterns are used, the LE method performs better than the Fourier method. When using more than 200 patterns, the residual error of the LE method becomes almost constant; this result makes sense because the LE method has small values of a_i for $i > 200$ (Fig. 5). The difference between the methods decreases when the number of bases becomes larger. This indicates that the LE basis is well suited to the reconstruction of the plasma.

Next, we evaluate the performance of the L_1 regularization method. Figure 7 shows a comparison of the coefficients of the L_1 and L_2 regularizations using the case of the LE basis using 1000 patterns. We can see that L_2 takes non-zero values across the entire range shown, whereas L_1 predominantly uses only lower-order patterns. In the L_1 method, 64.6% of coefficients are zero. This fact indicates that the L_1 regularization enables us to reconstruct the model using only the essential basis.

Figure 8 shows the results of reconstructions at two different times using experimental images utilizing the LE

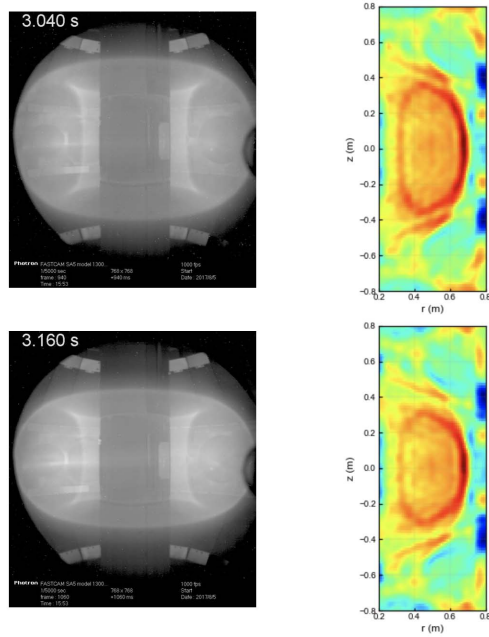


Fig. 8 Input camera images (left) and reconstructed images of the cross-sectional emissivity (right).

basis with 1000 patterns and the L_1 regularization. The left column is the image of QUEST taken from the tangential direction (input), and the right column is the reconstructed image (output). The upper row, taken at 3.040 s, is an unsteady state in which the coil current changes at every moment; the lower row, taken at 3.160 s, is taken in a steady state. We have been able to reconstruct the poloidal cross-sectional shape of the plasma boundary at both times.

4. MHD Equilibrium Calculation with TASK/EQU Code

In this section, we calculate the MHD equilibrium based on the estimated plasma surface from the reconstructed image. In doing so, we test the validity and effectiveness of the proposed method.

The plasma equilibrium in an experimental device is modelled using the theory of MHD equilibrium. MHD equations give an equation of motion of plasma:

$$\rho \frac{d\mathbf{v}}{dt} = \mathbf{j} \times \mathbf{B} - \nabla p + \rho \mathbf{g}. \quad (12)$$

Assuming steady-state in the MHD equation and ignoring the gravity term \mathbf{g} , Eq. (12) becomes

$$\nabla p = \mathbf{j} \times \mathbf{B}. \quad (13)$$

Using Maxwell's equations, we can derive the following Grad-Shafranov equation from Eq. (13). The poloidal flux function ψ of the plasma in the MHD equilibrium is described as follows:

$$\Delta^* \psi = \frac{\partial}{\partial R} \frac{1}{R} \frac{\partial}{\partial R} \psi + \frac{\partial^2 \psi}{\partial z^2} = -\mu_0 R j_\phi, \quad (14)$$

where j is the toroidal plasma current density, R is the radius in cylindrical coordinates, and z is parallel to the major axis. The current density satisfies the expression:

$$j_\phi = R p' + \frac{1}{\mu_0 R} F F', \quad (15)$$

where $F = B_\phi R$, B_ϕ is the toroidal magnetic field, and p is the plasma pressure. Both F and p are functions of ψ , (i.e. $p = p(\psi)$ and $F = F(\psi)$). The free-boundary equilibrium calculation code TASK/EQU [11] is used to solve Eq. (14) and thus to obtain the equilibrium magnetic field.

Here, we introduce the iterative solution of Grad-Shafranov equation, which is explained in Ref. [12] as the free-boundary equilibrium solver. The computational domain is a rectangular region with the axes R and z in cylindrical coordinates. The TASK/EQU code requires the boundary conditions, poloidal coil currents, and prescribed markers picked from the estimated plasma surface (the red curve in Fig. 9 (a)). The poloidal flux function can be decomposed into two elements:

$$\psi(R, z) = \psi_p(R, z) + \sum_i \psi_v^i(R, z), \quad (16)$$

where ψ_p is the contribution from the plasma current and ψ_v^i is that from the i -th poloidal coil. As Eq. (14) is a non-linear partial differential equation, the iterative solver is used as follows.

1. As an initial guess for $\psi_p(R, z)$, the Solov'ev [13] solution is used.
2. Adding the sum of ψ_v^i to ψ_p , the ψ distribution is obtained.
3. Using ψ distribution from step 2, the plasma current density j is calculated from Eq. (15).
4. Using the obtained j_ϕ , a new ψ_p distribution is calculated from Eq. (14).
5. With this ψ_p as an input to step 2, the process is repeated until the current distribution converges.

Note that ψ_v^i used in step 2 is determined for each iteration by the least-squares method with a penalty term of

$$W = \sum_j \left[\psi_p(R_j, z_j) + \psi_s + \sum_k I_{v,k} \psi_{v,k}(R_j, z_j) - \psi_j \right]^2 + \sum_k w_k \left[I_{v,k} - I_{v,k}^0 \right]^2, \quad (17)$$

where j indicates the j -th prescribed marker, k indicates the k -th poloidal coil, ψ_s is the poloidal flux function of the plasma surface, $I_{v,k}$ is the k -th coil current, $I_{v,k}^0$ is the prescribed coil current, ψ_j is the prescribed flux of the j -th marker and w_k is the weight. In this study, ψ_j is set $\psi_j = 0$ as a plasma surface point. The first term in the right-hand side makes the value of the flux function at the marker point closer to the input value. The second term makes the currents of each coil closer to the prescribed value. Therefore, the coil current is determined by the balance between

the prescribed marker condition and the initial coil current condition.

Figure 9(a) shows the selection of the prescribed markers. The selection process is as follows: First, points on the edge of emission intensity $f(r, z)$ are sampled as candidates for the location of the LCFS (orange and gray dots in Fig. 9(a)). This edge region is detected based on the Laplacian filter, which detects sharp intensity changes in the image and highlights the edges. The Laplacian value on the edge region satisfies the condition $\partial^2 f(r, z)/\partial r^2 + \partial^2 f(r, z)/\partial z^2 < -0.015$. These points are then clustered to the emission boundary group (orange dots) and other small groups (gray dots) using hierarchical clustering algorithm [14]. Next, as an estimate for the plasma surface, the Fourier series-expanded closed curve (red closed curve in Fig. 9(a)) is fitted to these points. The radius of this closed curve is then expanded to be 5% larger than the original fitted curve. Finally, the prescribed markers (blue X symbols in Fig. 9(a)) are picked from this closed curve. In this study, we made the simple assumption that the emitting surface and the LCFS are almost coincident; in reality, however, whether the emitting surface is inside or outside the LCFS depends on the electron temperature. In larger tokamaks including ITER with higher temperatures, the LCFS estimation algorithm needs to be calibrated according to the electron temperature.

The initial plasma parameters for calculation are given as follows: plasma density, $n_{e0} = 10^{17} \text{ cm}^{-3}$, electron temperature $T_{e0} = 10 \text{ eV}$, plasma pressure $p_0 = en_{e0}T_{e0} = 0.16 \text{ Pa}$, major radius $R = 0.5 \text{ m}$, toroidal magnetic field multiplied by major radius $RB_t = 0.16 \text{ m}\cdot\text{T}$.

Here, we discuss the rationale behind the utilization of

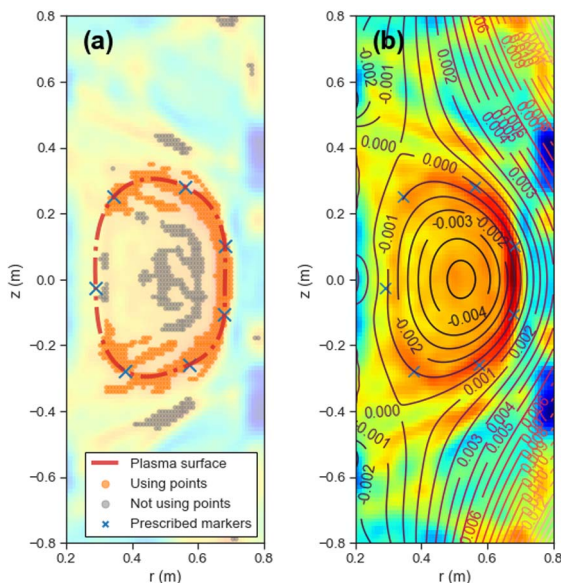


Fig. 9 (a) The procedure to estimate the tentative plasma surface. Blue X markers are used as prescribed markers in TASK/EQU. (b) The calculated contour of the magnetic flux.

the free-boundary equilibrium calculation code instead of the fixed-boundary code. In the fixed-boundary code (such as TASK/EQU), a prescribed LCFS is required as a boundary condition. The emission boundary of the reconstructed image has a finite width, and the closed curve of the LCFS cannot be defined precisely at first. Therefore, we sampled some likely points on the emission boundary from the obtained images and determined the LCFS by solving the GS equation together with the current information of poloidal coils.

A superposition of the reconstruction image and the calculated equilibrium field is shown in Fig. 9(b). The reconstructed local emissions are distributed just inside the separatrix (i.e. the LCFS) and almost on the single flux surface. Therefore, the reconstructed image and the computed magnetic field configuration are in good agreement; this indicates the validity of the proposed method. However, there is the difference between the prescribed marker positions and the LCFS. If the coil currents $I_{v,k}$ and the prescribed flux ψ_j in Eq. (17) are consistent, the LCFS will overlap the marker exactly. This problem can be solved by improving the accuracy of the reconstruction and the LCFS estimation algorithm.

5. Conclusions

We have proposed a tomographic method using tangential visible light for MHD equilibrium reconstruction via two processes.

The first process is the poloidal cross-section tomographic reconstruction to estimate the shape of the LCFS. Tomographic reconstruction consists predominantly of two parts. First, a target image, the poloidal cross-sectional emission profile, is expanded using orthogonal basis patterns. We have compared the Fourier and LE bases. The difference between these two methods of reconstruction is not significant when a sufficiently large number of bases are used. However, we have shown that the LE method performs well even when smaller number of bases are used. It is thus concluded that the LE basis is well suited to estimating plasma emissions. Second, we have introduced the L_1 regularization to solve the least-squares equation. It is found that the L_1 regularization makes many coefficients shrink toward zero. As a result, only essential patterns remain to reconstruct the image. This result aids reducing the noise.

The second process is the MHD equilibrium calculation using the free-boundary equilibrium calculation code, TASK/EQU. This code requires two types of boundary condition. One is the poloidal coil currents, and the second is the prescribed markers on the tomographically estimated plasma surface. The calculated contours of the magnetic flux show good agreement with the reconstructed image. A remaining issue is the difference between the estimated plasma surface and the calculated LCFS that is caused by the inconsistency between the estimated plasma

surface and the coil currents. This problem can be solved by improving the accuracy of the reconstruction and the LCFS estimation algorithm.

- [1] D.W. Swain and G.H. Neilson, Nucl. Fusion **22**, 1015 (1982).
- [2] J.L. Luxon and B.B. Brown, Nucl. Fusion **22**, 813 (1982).
- [3] L.L. Lao *et al.*, Nucl. Fusion **25**, 1611 (1985).
- [4] M. Anton *et al.*, Plasma Phys. Control. Fusion **38**, 1849 (1996).
- [5] Y. Nagayama, J. Appl. Phys. **62**, 2702 (1987).
- [6] K. Yamasaki *et al.*, Rev. Sci. Instrum. **88**, 093507 (2017).
- [7] S. Ohdachi *et al.*, Plasma Fusion Res. **14**, 3402087 (2019).
- [8] K. Hanada *et al.*, Plasma Fusion Res. **5**, S1007 (2010).
- [9] R. Tibshirani, J. R. Statist. Soc. B **58**, 267 (1996).
- [10] B. Efron, T. Hastie, I. Johnstone and R. Tibshirani, Ann. Statist. **32**, 407 (2004).
- [11] A. Fukuyama and M. Yagi., Plasma Fusion Res. **81**, 747 (2005) in Japanese.
- [12] M. Honda, Comput. Phys. Commun. **181**(9) 1490 (2010).
- [13] L.S. Solov'ev, JETP **26**, 400 (1968).
- [14] F. Murtagh and P. Contreras, Algorithms for hierarchical clustering: an overview. WIREs Data Min Knowl Discov2011; **2**: 86-97.